11th World Congress on Computational Mechanics (WCCM XI)
5th European Conference on Computational Mechanics (ECCM V)
6th European Conference on Computational Fluid Dynamics (ECFD VI)
E. Oñate, J. Oliver and A. Huerta (Eds)

COMPUTATION OF LAMINAR AND TURBULENT WATER HAMMER FLOWS

S. D. SAEMI[1, 2], M. RAISEE[1, 2], M. J. CERVANTES[3] AND A. NOURBAKHSH[1, 2]

[1]Hydraulic Machinery Research Institute (HMRI), School of Mechanical Engineering
College of Engineering, University of Tehran, P. O. Box: 11155-4563, Tehran, Iran.

[2]Center of Excellence in Design and Optimization of Energy Systems (CEDOES)
School of Mechanical Engineering, College of Engineering, University of Tehran,
P.O.Box: 11155-4563, Tehran, Iran.
si.saemi@ut.ac.ir

[3] Division of Fluid and Experimental Mechanics,
Luleå University of Technology, SE 971 87, Lulea, Sweden.
Michel.Cervantes@ltu.se

Key Words: *Water hammer, laminar flow, turbulent flow, numerical simulation.*

Abstract. In this paper, the water hammer phenomenon in a pipeline is simulated using the full Reynolds-Averaged Navier-Stokes equations. The flow is considered to be compressible and the effect of pipe elasticity is taken into account by introducing the bulk modulus of elasticity in the solution procedure. Computations are performed both for laminar and turbulent flows. The high-Re RNG k-ε and the low-Re k-ω SST turbulence models are employed for turbulence modeling. Numerical results for both laminar and turbulent flows are compared with the available experimental data and numerical results in the literature. For the laminar flow test case, the head variation shows good agreement with the experimental data. Comparisons for turbulent test case show that the RNG k-ε model somewhat overpredicts the head variation. The low-Re k-ω SST model, in the other hand, produces more accurate wall shear stress distribution than the high-Re RNG k-ε model. This highlights the importance of implementation of low-Re turbulence models for the prediction of water hammer flows.

1 INTRODUCTION

The term ‘water hammer’ is used to describe the fluid flow characteristics when a fluid in motion is forced to stop in closed systems such as a pipe network. This phenomenon produces intense pressure waves that travel periodically along the pipe. Water hammer mostly occurs in piping systems, e.g., in power plants and urban water carrier systems, due to a sudden change in the flow rate during a sudden closure (or opening) of a valve or pump failure involving a density variation. Many researchers have used experimental as well as theoretical methods to examine the phenomena of the water hammer in straight pipes. An example of experimental works is the study of Holmboe et al. [1] who measured the pressure variation in transient laminar flow and compared the results with frictionless analysis of Joukowski [3]. It was shown that the theoretical solution considering inviscid flow is valid when low viscous liquid like water is employed in the measurements. Bergant et al. [2] measured the pressure

variation, caused by fast closure of the valve, in laminar and low Reynolds turbulent flows. Safwat [6] measured the strains in the pipe wall, resulting from fast closure of the valve, to evaluate the elastic behavior of the pipe during the water hammer. They concluded that, the strain measurement on the outer side surface of the pipe wall can yield indirectly the transient pressure changes in the pipe. Brunone et al. [7] measured pressure and velocity profiles caused by water hammer and compared the measured pressure change with the results of 1D simulation. Concerning analytical studies, one can refer to the work of Joukowsky [2] who proposed the following well-known formula for the piezometric pressure which is called 'fundamental equation of water hammer'.

$$\Delta H = \pm \frac{a \Delta u}{g} \tag{1}$$

where a, H and u are respectively the wave speed, the piezometric head and the cross sectional average velocity. Ghidaoui and Kolyshkin [8] performed a linear stability analysis for the velocity profiles in both unsteady laminar and turbulent flows caused by water hammer. They demonstrated that the sources of flow instability are the presence of inflection points in the velocity profile and large gradient near the pipe wall.

One of the main issues in water hammer modeling is the application of reliable unsteady friction models for predictions. Therefore, a number of researches performed experimental and analytical investigations to develop accurate unsteady friction models. Among the proposed models for 1D simulation of water hammer, the Darcy-Weisbach shear stress for head losses in turbulent pipe flow is the most well-known model. This model is based on steady axial averaged velocity but remains valid under unsteady condition [9].

$$\tau_w = \rho f \frac{u|u|}{8} \tag{2}$$

As reported in Ghidaoui et al. [10], the application of this model in very slow transient flows (quasi-steady) gives acceptable results. However, water hammer flow occurs in very fast transient conditions. To address this issue, the unsteady wall shear stress τ_{wu} is introduced as:

$$\tau_{wu} = \tau_w - \tau_{ws} \tag{3}$$

The unsteady wall shear stress has been modeled using empirical-based corrections on quasi-steady shear stress models derived from laboratory experiments by Brunone et al [5], Pezzinga [11] and Bergant et al [2] as well as physically based models which are based on analytical solutions of the unidirectional flow used in 1D water hammer simulations. Among the physically based models, the Zielke model [4] derived from the Laplace transform of the axial component of the Navier-Stokes equations in laminar regime, is the most well-known one. Bergant et al [2] and Trikha [12] employed Zielke model [4] to simulate turbulent transient pipe flows and found that this model is applicable for low Reynolds turbulent transient flows. Also the Vardy and Brown model [13, 14] is widely used for turbulent transient flows in smooth and rough pipes by frozen turbulence model assumption. Due to the limitations in obtaining detailed information in 1D simulations, e.g. velocity and pressure fields and energy dissipation, 2D simulation using appropriate turbulence models should be performed. The most widely used turbulence models in the literature are algebraic turbulence

models due to their simple mathematical formulation. Examples of application of algebraic turbulence models for the prediction of water hammer problem are two-layer turbulence model of Cebeci-Smith [15], five-region turbulence model of Kita et al. [16] and Baldwin and Lomax [17]. More recently, Riasi et al. [24] used the Wilcox k-ω model to study water hammer in a pipe.

Concerning the numerical methods used for the water hammer simulations, the most widely used numerical scheme is the method of characteristics (MOC) introduced by Wylie et al. [25] and Chaudhry [26] due to its simple numerical implementation and efficiency as well as its ability to handle complex boundary conditions. This method transforms partial differential equations into ordinary differential equations along characteristics lines. Integrating from one time step to the next requires pressure and velocity to be known along each characteristics line. As shown by Tijsseling et al. [27], the MOC method gives an accurate prediction of the maximum pressure in the system which usually occurs during the first pressure peak. It also correctly predicts wave periods, though it usually fails in the prediction of damping and dispersion of wave fronts accurately. Chaudhry and Husssaini [28] used MacCormack, Lambda and Gabutti explicit finite difference schemes to solve the water hammer equations. Their work shows that the second order finite difference method (in time and space) produces more accurate results than the first order MOC with courant number less than one. Another important numerical method in the solution of water hammer hyperbolic system of equations is the finite volume method. This method has some profits such as the conservative character and the ability to provide the correct resolution of discontinuities resulting from the pressure changes. This method was first used by Guinot [29] who employed the two-dimensional Riemann solver. Moreover, Zhao and Ghaidaoui [30] implemented first- and second-order explicit finite volume Godunov-type solution for water hammer simulation. They indicated that the second order methods produce more accurate results than the first order ones. All of the studies described in the literature relied on simplified water hammer equations for predictions and did not use full Navier-Stokes equations.

For more precise prediction of the water hammer phenomena in complex 3D geometries, one requires to employ full governing equations. For this purpose, in this work, we investigated the water hammer in a straight pipe based on unsteady Reynolds averaged Navier-Stokes (URANS) equations using finite volume method and without any change in the nature of the governing equations. The CFD-based simulations of water hammer are performed using FLUENT software. The simulations are conducted for both laminar and turbulent flows. The high-Re RNG k-ε and the low-Reynolds k-ω SST turbulence models are employed for the predictions. The predicted pressure head at the pipe centreline midpoint are compared with the available experimental data.

2 PROBLEM DESCRIPTION AND MATHEMATICAL FORMULATION

2. 1 Test cases

The geometry considered for the water hammer simulations is shown in Fig. 1 and the details of experiments are summarized in Table 1. As indicated in Table 1 computations of the present work have been carried out for both laminar and turbulent water hammer flows. The experimental work for the laminar test case was performed at Reynolds number of 82 by Holmboe et al [1]. In order to get water hammer, a fast closing valve is located at the end of a

1" ID copper tube. The pipe is placed in concrete to damp the vibration created by the water hammer. A 60 gallons capacity tank is utilized to have an infinite reservoir at the other end of the tube. The tank pressure maintained constant by the use of compressed air and pressure transducers were used to measure the head change in various locations. As described in Bergant et al. [2], the turbulent experimental test case contains a flexible laboratory apparatus involving a long copper pipe of 22.1 mm in diameter connected to two pressurized tanks. The pressure of the two tanks was specified and controlled by computerized pressure control system. The water hammer in the apparatus was initiated by the rapid closure of a ball valve. In both experimental works the pressure change at the end and in the middle of the pipe was measured.

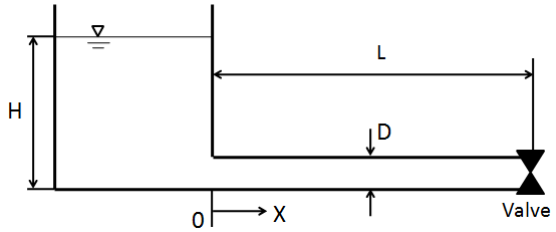

Fig. 1: Pipe geometry used for the water hammer simuations.

The numerical simulations were performed with a 2D geometry shown in Fig. 1 assuming an axis-symmetric flow.

Table 1: The details of the test cases

Test No.	Pipe length (m)	Pipe diameter (m)	Density (kg/m^3)	Wave velocity (m/s)	Initial velocity (m/s)	Dynamic viscosity (N s/m^2)	Reynolds Number (-)
1	36.09	0.025	878.4	1324	0.13	0.03483	82
2	37.2	0.022	998.2	1276	0.3	0.0011545	5700

2. 2 Governing equations

For compressible laminar and turbulent flows, the conservation laws of mass and momentum may be written as follows:
Continuity:

$$\frac{\partial \rho}{\partial t}+\frac{\partial(\rho u_j)}{\partial x_j}=0 \tag{4}$$

Momentum:

$$\frac{\partial(\rho u_i)}{\partial t}+\frac{\partial(\rho u_j u_i)}{\partial x_j}=-\frac{\partial P}{\partial x_i}+\frac{\partial}{\partial x_j}\left(\mu\frac{\partial u_i}{\partial x_j}-\rho\overline{u_i' u_j'}\right) \tag{5}$$

It should be noted that the Reynolds stress term in Eq. (5) vanishes in the laminar flow. To account for the effect of pipe elasticity a new Bulk modulus of elasticity $K_f' = K_f \big/ \left(1+K_f D/eE\right)$ is introduced. A rigid pipe assumption will give rise to a change of pressure larger than for an elastic one. This leads to a higher wave speed which is incompatible with the experimental

data. Introducing a new Bulk modulus based on the change of pipe diameter is appropriate to solve the water hammer phenomenon. The pressure wave speed is thus given by:

$$a = \sqrt{\frac{K_f / \rho}{1 + K_f D / eE}} \tag{6}$$

Where K_f is the bulk modulus of elasticity of the fluid, E is the Young modulus of elasticity, e is the thickness of the pipe, D is the diameter of the pipe and ρ is the density of the fluid. The flow is assumed to be compressible and isothermal. Thus, the density variation depends only on the pressure change and is computed based on the following equation:

$$d\rho = \rho dp / K_f' \tag{7}$$

This equation provides the relationship between the pressure and the density change and implemented by a User Defined Function (UDF) into the FLUENT software.

2. 3 Turbulence modeling equations

In order to simulate turbulent water hammer, the high-Re RNG k-ε and the low-Re k-ω SST turbulence models were used for the computations. The mathematical formulation of the RNG k-ε model is similar to the standard k-ε but with some modifications [31]. The wall functions approach is used to simulate the flow with the RNG k-ε model. The k-ω SST model is suitable for the prediction of turbulent flows with the pressure gradient

2. 3. 1 The high-Re RNG k-ε turbulence model

In the high-Re RNG k-ε turbulence model, the Reynolds stress tensor in the momentum Eq. (5) is modeled by the eddy viscosity approximation:

$$-\overline{u_i' u_j'} = \nu_t \left(\frac{\partial u_i}{\partial x_j} + \frac{\partial u_j}{\partial x_i} \right) - \frac{2}{3} \delta_{ij} k \tag{8}$$

where k is the turbulent kinetic energy and ν_t is turbulent kinematic viscosity, which is defined as:

$$\nu_t = C_\mu \frac{k^2}{\varepsilon} \tag{9}$$

To obtain ν_t, the following transport equations are solved for the turbulent kinetic energy and its dissipation rate:

$$\frac{\partial}{\partial t}(\rho k) + \frac{\partial}{\partial x_j}(\rho k u_j) = \frac{\partial}{\partial x_j}\left(\left(\mu + \frac{\mu_t}{\sigma_k} \right) \frac{\partial k}{\partial x_j} \right) + P_k - \rho \varepsilon \tag{10}$$

$$\frac{\partial}{\partial t}(\rho \varepsilon) + \frac{\partial}{\partial x_j}(\rho u_j \varepsilon) = \frac{\partial}{\partial x_j}\left[\left(\mu + \frac{\mu_t}{\sigma_\varepsilon} \frac{\partial \varepsilon}{\partial x_j} \right) \right] + C_{\varepsilon 1} \frac{\varepsilon P_k}{k} - C_{\varepsilon 2}^* \rho \frac{\varepsilon^2}{k} \tag{11}$$

where P_k is the turbulent energy production. $C_{2\varepsilon}^{*} = C_{2\varepsilon} + C_{\mu}\eta^3\left(1-\eta/\eta_0\right)\Big/\left(1+\beta\eta^3\right)$ and $\eta = S\,k/\varepsilon$ with $S = \left(2S_{ij}S_{ij}\right)^{1/2}$. All model constants are given in Table 2.

Table 2: Empirical constants for the k-ε model

C_{μ}	$C_{\varepsilon 1}$	$C_{\varepsilon 2}$	σ_k	σ_{ε}	η_0	β
0.0845	1.42	1.68	0.7194	0.7194	4.38	0.012

2. 3. 2 The low-Re k-ω SST model

In the low-Re k-ω SST model, the unknown Reynolds stress tensor is also obtained from the Boussinesq approximation (Eq. 8). The k-ω SST model uses the original k-ω model of Wilcox in the inner region and the standard k-ε in the outer region of the boundary layer which overcomes the strong sensitivity of the Wilcox model to the free stream conditions [32]. In this model the eddy viscosity ν_t is obtained from:

$$\nu_t = a_1 k \big/ \max\left(a_1\omega, \Omega F_2\right) \tag{12}$$

where Ω is the absolute value of vorticity. Moreover, the turbulent kinetic energy, k, and its specific dissipation, ω, are obtained from the following equations:

$$\frac{\partial}{\partial t}(\rho k) + \frac{\partial}{\partial x_j}\left(\rho k u_j\right) = \frac{\partial}{\partial x_j}\left(\left(\mu + \sigma_{k1}\mu_t\right)\frac{\partial k}{\partial x_j}\right) + P_k - \beta^{*}\rho k\omega \tag{13}$$

$$\frac{\partial}{\partial t}(\rho\omega) + \frac{\partial}{\partial x_j}\left(\rho u_j \omega\right) = \frac{\partial}{\partial x_j}\left[\left(\mu + \sigma_{\omega 1}\mu_t\right)\frac{\partial \omega}{\partial x_j}\right] + \frac{\gamma}{\nu_t}P_k - \beta\rho\omega^2 + 2\left(1-F_1\right)\rho\sigma_{\omega 2}\frac{1}{\omega}\frac{\partial k}{\partial x_j}\frac{\partial \omega}{\partial x_j} \tag{14}$$

$$F_1 = \tanh\left\{\left\{\min\left[\max\left(\frac{\sqrt{k}}{\beta^{*}\omega y}, \frac{500\nu}{y^2\omega}\right), \frac{4\sigma_{\omega 2}k}{CD_{k\omega}y^2}\right]\right\}^4\right\} \tag{15}$$

In order to obtain the model constants of the k-ω SST, ϕ_1 is considered as any constant in the original model (Wilcox k-ω model) and ϕ_2 as any constant in the transformed model (standard k-ε model). Then, the constants are obtained via $\phi = \phi_1 F_1 + \phi_2\left(1-F_1\right)$. The parameter F_1 is designed to be one in the near wall region which activates the original model and zero away from the surface. The constants for the k-ω SST model are given in Table 3. The production term is defined as:

$$P_k = \min\left(\tau_{ij}\frac{\partial u_i}{\partial x_j}, 10\beta^{*}k\omega\right) \tag{16}$$

where τ_{ij} is the turbulent shear stress term defined by Eq. (8). F_2 is a function that is respectively zero for free shear layer and one for boundary layer flows.

$$F_2 = \tanh\left[\left[\max\left(\frac{2\sqrt{k}}{\beta^* \omega y}, \frac{500\nu}{y^2\omega}\right)\right]^2\right] \tag{17}$$

$CD_{k\omega}$ is the positive portion of the cross diffusion term.

$$CD_{k\omega} = \max\left(2\rho\sigma_{\omega 2}\frac{1}{\omega}\frac{\partial k}{\partial x_i}\frac{\partial \omega}{\partial x_i}, 10^{-10}\right) \tag{18}$$

All the computations have been carried out using the FLUENT software. The SIMPLE algorithm was used for the calculation of the pressure field. Furthermore, the nonlinear convective term in all transport equations was approximated using the MUSCL third-order scheme. The first-order implicit scheme was employed for the discretization of the time derivative terms.

Table 3: Empirical constants for the k-ω models

α_1	α_2	β_1	β_2	β^*	σ_{k1}	σ_{k2}	$\sigma_{\omega 1}$	$\sigma_{\omega 2}$
5/9	0.44	3/4	0.0828	0.09	0.85	1	0.5	0.856

To ensure the accuracy of the results, three different grid sizes were investigated using the k-ω SST turbulence model, see Table 4. The grids in radial direction are clustered near the wall but in the axial direction are uniformly distributed. As shown in Fig. 2, computations in all three grids resulted in similar pressure variations. The second mesh with (40×1000) grid nodes was selected for the turbulent flow simulations. For the laminar case, a computational grid consisting of 3000×18 nodes in the axial and radial directions was selected.

Table 4: Number of grids

Case No.	No. of Grids: (radial × axial)
1	20×500
2	40×1000
3	60×2000

To simulate water hammer phenomena due to the sudden valve closure, first steady state computations were performed using the pressure inlet and the pressure outlet boundary conditions. When the solution converged, the pressure outlet boundary condition was switched to the wall boundary condition and the simulation continued with the unsteady scheme. The time step of the transient solution was 10^{-4} sec.

3. 1 Laminar water hammer

The numerical results for the laminar water hammer are presented in Figs. 3 and 4. As clearly seen in Fig. 3, the computed distribution of head at the mid-point between inlet and outlet of the pipe is in excellent agreement with the experimental data of Holmboe et al. [1]. It can be seen that at $0<t<0.7L/a$, the pressure head does not change with time. This means that the pressure wave still does not reach the mid-section of the pipe. At $t=0.7L/a$, the wave reflected from the valve passes the midpoint and rises the head pressure. At $t=1.7L/a$, the pressure wave reflected from the reservoir passes from the midpoint and thus reduces the head. By

increasing the time, at t=2.7L/a, the wave reflected from the valve passes the midpoint. In this condition, the head reduces to minimum level. Finally, at t=4L/a, the second reflected wave from the reservoir passes the midpoint which is an initial condition for the second wave cycle. Fig. 4 shows the variation in the velocity profile at the mid-section at different times. The results are in agreement with Wahba [21] numerical simulations, who simulated the same case using the forth order Runge-Kutta scheme for the temporal discritization and the second order central difference method for the spatial derivatives. It can be seen that at t=0 the velocity profile is similar to the fully-developed velocity profile. By traveling the wave in a reciprocating manner, the velocity magnitude changes with time. However, in all cases, away from the wall, the velocity profile keeps its original shape. It should be mentioned that Wahba [21] solved water hammer equations in their work while here we use the full Navier-Stokes equations.

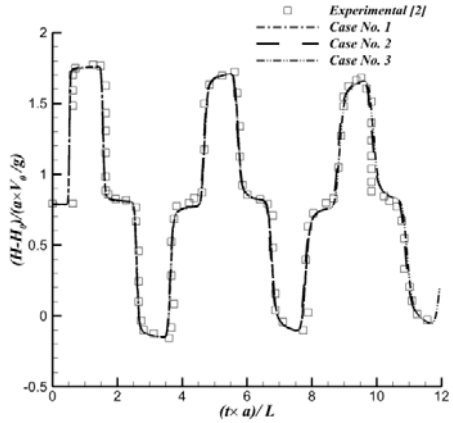

Fig. 2: The pressure head based on three grid numbers

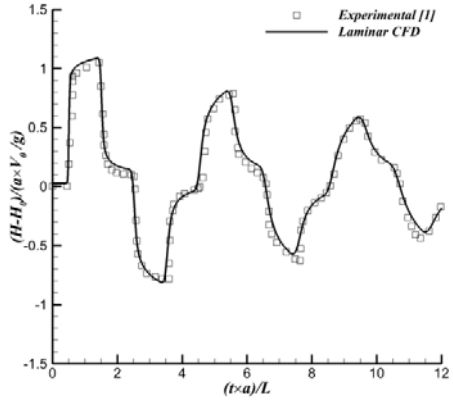

Fig. 3: Head of the flow at the mid-section as a function of time, Experimental: Experimental results of Holmboe et al. [1] , L: pipe length, a: speed velocity, V_0: initial water velocity

The distribution of the wall shear stress for the laminar flow is shown in Fig. 5. The peaks in the shear stress occur as the wave passes from the selected location. In between, the shear stress reduces to a new steady condition.

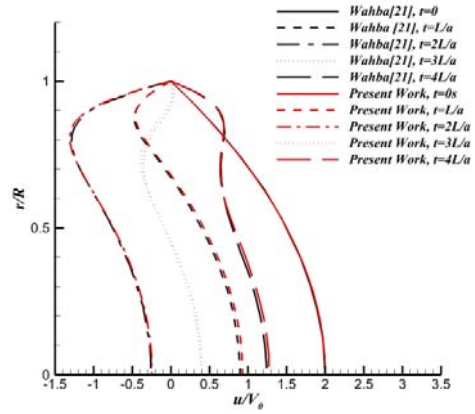

Fig. 4: The change of velocity profile at mid section as a function of time, V_0 initial water velocity, R pipe radius

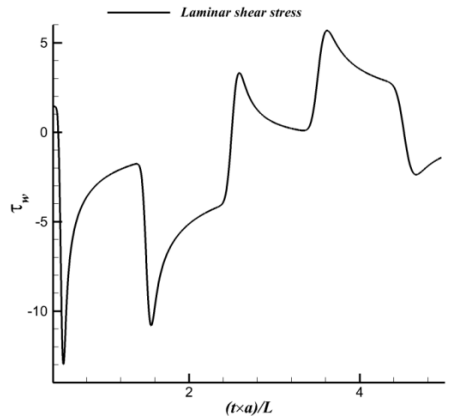

Fig. 5: Shear stress variation on the wall, L: pipe length, a: speed velocity, V_0: initial water velocity

3. 2 Turbulent water hammer

In Fig. 6, the time history of head is compared with the experimental data of Bergant et al. [2] at mid-point between the inlet and outlet of the pipe. While results of both turbulence models are more or less similar, the head predictions of the low-Re SST k-ω model are in better agreement with the experimental data. Note that the second and third peaks in the head distribution are somewhat overpredicted by the high-Re RNG k-ε model, but well captured by the low-Re k-ω SST model.

In Fig. 7, the predicted velocity profiles at the mid-section of the pipe are compared with the numerical results of Zhao et al. [22] who used the low-Re k-ε turbulence model of Fan et al. [23] for simulations. As expected, the RNG k-ε model with wall functions is unable to capture the variation of the velocity profile close to the wall. The main difference between the laminar and turbulent cases lies in the near wall behavior of the flow. The strength of the reverse flow is stronger in the turbulent flow. Moreover, the region of the reversed flow in the turbulent flow is confined to a smaller region at the pipe wall.

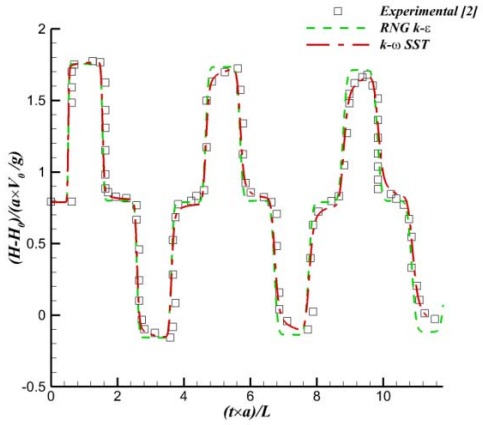

Fig. 6: Head of the flow at the mid-section as a function of time, Experimental [2]: Experimental data of Bergant et al., – – – – Numerical Simulation with RNG k-ω Turbulence model, – – – – Numerical simulation with k-ω SST turbulence model, L: pipe length, a: wave speed , V_0: initial water velocity

Fig. 8 shows the wall shear stress distribution at the mid-section of the pipe. It is seen that the RNG k-ε model is unable to capture the wall shear stress variation correctly which is due to the use of wall functions.

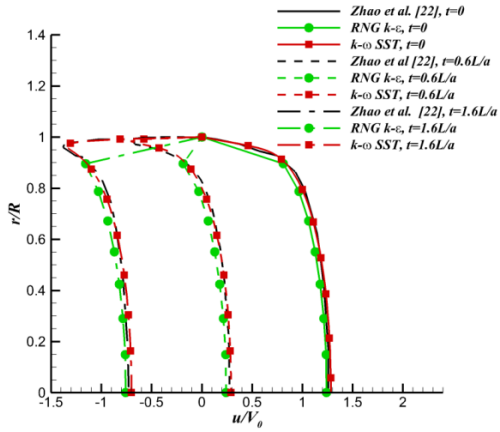

Fig. 7: The change of velocity profile at the mid-section as a function of time, Zhao et al. [22]: Numerical simulation of Zhao et al., ● Numerical Simulation with RNG k-ε Turbulence model, ■ Numerical simulation with k-ω SST turbulence model. V_0 initial water velocity, R pipe radius

4 CONCLUSIONS

It this paper, the full Navier-Stokes equations are used to simulate water hammer phenomenon in the laminar and turbulent regimes. The numerical results for both test cases are found to be in excellent agreement with the reported experimental data in the literature. For the turbulent water hammer, the results of low-Re k-ω SST turbulence model are found to be in better agreement with the experimental data. The velocity profiles tend to maintain their initial shape except near the wall. The velocity profiles show a strong reverse flow near the pipe wall which is stronger in the turbulent flow. Further 3D computations should be performed to consider the effects of valve closure on the predictions.

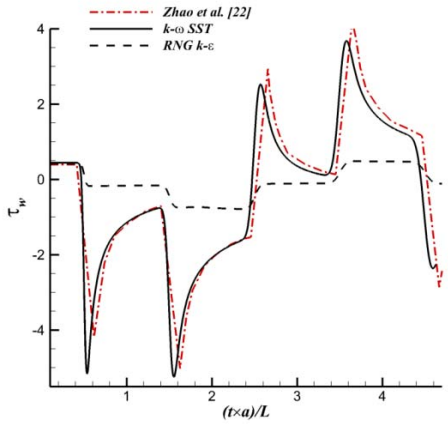

Fig. 8: Shear stress variation on the wall, Zhao et al. [22]: Numerical simulation of Zhao et al., L: pipe length, a: speed velocity, V_0: initial water velocity

5 ACKNOWLEDGMENTS

The authors wish to thank University of Tehran (UT) and Luleå University of Technology (LUT) for providing financial support of this work.

6 REFERENCES

[1] Holmboe, EL., Rouleau, WT., 1967, The effect of viscous shear on transients in liquid lines, Journal of Basic Engineering, Transactions of the ASME, Vol. 89, No. 1, pp. 174–180.
[2] Bergant, A., Simpson, A. R., and Vitkovsky, J., 2001, Developments in Unsteady Pipe Flow Friction Modelling, J. Hydraul. Res. Vol. 39, No. 3, pp. 249–257.
[3] Joukowski, N., 1904, Water Hammer, translated by Miss O. Simin, Proceedings of American TFnier TForA's Assoc., Vol. 24, pp. 365 -368.
[4] Zielke, W., 1968, Frequency-dependent friction in transient pipe flow, J. Basic Eng., Vol. 90, No. 1, pp. 109–115.
[5] Brunone, B., Golia, U. M., and Greco, M., 1991, Some Remarks on the Momentum Equation for Fast Transients, Proc. Int. Conf.on Hydr. Transients with Water Column Separation, IAHR, Valencia, Spain, pp. 201–209.
[6] Safwat, H., 1972, On the Elastic Behavior of the Pipe Wall for Water Hammer Applications, Nuclear Engineering and Design, pp. 85-94.
[7] Brunone, B., Karney, B. W., Mecarelli, M., Ferrante, M., 2000, Velocity Profiles and Unsteady Pipe Friction in Transient Flow, J. of Water Resources Planning and Management, pp. 236-244.
[8] Ghidaoui, M. S., and Kolyshkin, A. A., 2001, Stability Analysis of Velocity Profiles in Water-Hammer Flows, Journal of Hydraulic Engineering, Vol. 127, No. 6, pp. 499–512.
[9] Streeter, V. L. and Wylie, E. B., 1985, Fluid Mechanics, 8th Edition, McGraw Hill New York.
[10] Ghidaoui, M., Zhao, M., Mclnnis, D. A., Axworthy, D. H., 2005, A Review of Water Hammer Theory and Practice, Journal of Applied Mechanics Review, Vol.58, No.1, pp.49-76.
[11] Pezzinga, G., 2000, Evaluation of unsteady flow resistances by quasi-2D or 1D models, J Hydr. Engng., Vol. 126, No. 10, pp. 778–785.

[12] Trikha, A. K., 1975, An efficient method for simulating frequency-dependent friction in transient liquid flow, Journal of Fluid Engineering, ASME, Vol. 97, No. 1, pp. 97–105.
[13] Vardy, A. E., and Brown, J. M. B., 2003, Transient Turbulent Friction in Smooth Pipe Flows, J. Sound and Vibration, Vol. 259, No. 5, pp. 1011-1036.
[14] Vardy, A. E., and Brown, J. M. B., 2004, Transient Turbulent Friction in Rough Pipe Flows, J. Sound and Vibration, Vol. 270, pp. 233-257.
[15] Cebeci, T., Smith, A. M. O., 1974, Analysis of turbulent boundary layers, Academic Press, NewYork.
[16] Kita, Y., Adachi, Y., Hirose, K., 1980, Periodically oscillating turbulent flow in a pipe, Bulletin JSME, Vol. 23, No. 179, pp. 656–664.
[17] Baldwin, B.S., Lomax, H., 1978, Thin layer approximation and algebraic model for separated turbulent flows, AIAA Paper, pp. 78–257.
[18] Vardy, A. E., Hwang, K. L., 1991, A characteristic model of transient friction in pipes, J. Hydr. Res., Vol. 29, No. 5, pp. 669–685.
[19] Silva-Araya, W. F., Chaudhry, M. H., 1997, Computation of Energy Dissipation in Transient Flow, Journal of Hydraulic Engineering, American Society of Civil Engineers, Vol. 123, pp. 108–115.
[20] Zhao, M., Ghidaoui, M.S., 2003, Efficient quasi two-dimensional model for water hammer problems, J. Hydr. Engng., Vol. 129, No. 12, pp. 1007–1013.
[21] Wahba, E. M., 2006, Runge-Kutta Time-Stepping Schemes with TVD Central Differencing for the Water Hammer Equations, Int. J. Numerical Methods in Fluids, Vol. 52, pp. 571-590.
[22] Zhao, M., Ghidaoui, M. S., 2006, Investigation of Turbulence Behavior in Pipe Transient Using a k-ε Model, J. of Hydraulic Research, Vol. 44, No. 5, PP. 682-692.
[23] Fan, S., Lakshminarayana, B., and Barnett, M., 1993, Low-Reynolds-Number Model for Unsteady Turbulent Boundary-Layer Flows, AIAA J., Vol. 31, No. 10, pp. 1777–1784.
[24] Riasi, A., Nourbakhsh, A., Raisee, M., 2009, Unsteady turbulent pipe flow due to water hammer using k-ω turbulence model, J. of Fluids Engineering, Vol. 47, No. 4, pp. 429-437.
[25] Wylie, E. B., Streeter, V. L., and Lisheng, S., 1993, Fluid Transient in Systems, Prentice-Hall, Englewood Cliffs.
[26] Chaudhry, M. H., 1987, Applied Hydraulic Transients, Van Nostrand Reinhold, N Y.
[27] Tijsseling, A. S, Lambert, M. F., Simpson, A. R., Stephens M. L., Vítkovský, J. P., Bergant, A., 2008, Skalak's extended theory of water hammer, Journal of Sound and Vibration, Vol. 310, No. 3, pp. 718-728.
[28] Chaudhry, M. H., and Hussaini, M. Y., 1985, Second-order accurate explicit finite-difference schemes for water hammer analysis, J. Fluids Eng., Vol. 107, pp. 523–529.
[29] Guinot, V., 2002, Riemann Solvers for Water Hammer Simulations by Godunov Method, Int. J. Numer. Methods Eng., Vol. 49, pp. 851–870.
[30] Zhao, M., Ghidaoui, M., 2004, Godunov-Type Solutions for Water Hammer Flows, Journal of Hydraulic Engineering, Vol. 130, pp. 341-348.
[31] Yakhot, V., Orszag, S.A., Thangam, S., Gatski, T.B. & Speziale, C.G., 1992, Development of turbulence models for shear flows by a double expansion technique, Physics of Fluids A, Vol. 4, No. 7, pp1510-1520.
[32] Menter, F. R., 1994, Two-Equation Eddy-Viscosity Turbulence Models for Engineering Applications, AIAA Journal, Vol. 32, No 8. pp. 1598-1605.